

Double-action dark matter, PAMELA and ATIC

Kingman Cheung^{1,2,3}, Po-Yan Tseng¹, and Tzu-Chiang Yuan⁴

¹*Department of Physics, National Tsing Hua University, Hsinchu 300*

²*Physics Division, National Center for Theoretical Sciences, Hsinchu 300*

³*Division of Quantum Phases & Devices,*

School of Physics, Konkuk university, Seoul 143-701, Korea

⁴*Institute of Physics, Academia Sinica, Nankang, Taipei 11529, Taiwan*

(Dated: April 7, 2009)

Abstract

Motivated by a two-bump (or 1-peak plus 1-hump) structure in the ATIC data, we perform a statistical analysis fitting the PAMELA and ATIC data to a dark matter model, in which the dark matter particle can undergo both annihilation and decay. Using a chi-square analysis we show that both data can be simultaneously fitted better with such a double-action dark matter particle. We use an existing neutrino mass model in literature to illustrate the idea.

I. INTRODUCTION

The year 2008 had been filled with excitement from a number of dark matter (DM) experiments. The PAMELA Collaboration [1] has reported an unexpected rise of positron fraction at the energy range of $10 - 100$ GeV, unlike the power-law falling background. This provides further support to the earlier results reported from HEAT [2] and AMS-1 [3]. However, similar enhancement of the anti-proton flux was expected but not seen by PAMELA [4] provides a challenging puzzle. Other surprises came from two balloon experiments ATIC [5] and PPB-BETS [6] at the South Pole Antarctica. The ATIC data showed an excess of galactic cosmic-ray electrons/positrons at energies of $300 - 800$ GeV. These experimental results have stimulated a lot of theoretical speculations about possible mechanisms, including dark matter annihilation [7], decaying dark matter with a very long lifetime [8], or simply astrophysical origins from either ultrahigh energy cosmic rays [9] or nearby pulsars [10] within a few kilo-parsec. If the observed positron excess is indeed due to dark matter annihilation, the data sets require an annihilation cross section $\langle\sigma v\rangle$ of the order of $10^{-23} \text{ cm}^3 \text{ s}^{-1}$, which is two to three order of magnitudes larger than naively expected from a thermo-WIMP dark matter in most popular models like the minimal SUSY and Kaluza-Klein models. Either a large boost factor or Sommerfeld-type enhancement [11] can be used to explain such a large annihilation cross section. On the other hand, a very long lifetime of the decaying dark matter of the order of 10^{26} seconds is required to fit the data. Such a long-lived dark matter is consistent with other cosmological constraints on our Universe. Implications for further investigations in future gamma-ray experiments and neutrino telescopes have been studied [12].

We point out that the excess in the ATIC data in fact consists of 1-peak plus 1-hump structure. The peak is from $300 - 800$ GeV while the bump from $80 - 300$ GeV. A possible explanation is that the dark matter particle in the Universe undergoes both annihilation and decay. The annihilation gives rise to the peak around 600 GeV while the decay is responsible for the small bump around $80 - 300$ GeV. The resulting positron fraction observed at PAMELA is a combination of annihilation and decaying contributions.

In this work, we perform a χ^2 analysis which shows that the fitting using a single mode (either annihilation or decay) is far less satisfactory than the double mode (both annihilation and decay). The study shows that a dark matter particle of about 640 GeV with a

monochromatic annihilation spectrum and a soft decaying spectrum is the best simultaneous fit to the PAMELA and ATIC data.

The PAMELA data is highly restrictive on the anti-proton mode of the dark matter annihilation or decay [4]. It points to the hint that the dark matter particle may be leptophilic or carrying a lepton number. There are some models that propose the TeV right-handed neutrino, which is responsible for neutrino mass, to be the dark matter candidate. We will borrow an example in literature [13, 14, 15] to illustrate the possibility.

Some of the highlights in this paper include

- We show in a more quantitative way how the models are fitted to the ATIC and PAMELA data simultaneously;
- We use the MINUIT program from the CERN library to vary the parameters of the model to minimize the χ^2 in order to obtain the best fit of the model;
- We show that the dark matter candidate that can both annihilate and decay can fit better to the data.

The organization of the paper is as follows. In the next section, we summarize the formulae we employed in our analysis for the annihilation and decay of the dark matter particle without referring to any particular dark matter models. In Sec. III, we show our numerical analysis of χ^2 fits. In Sec. IV, we describe a slight modification of an existing dark matter model in literature that may give rise to the double-action. We conclude in Sec. V.

II. DOUBLE-ACTION DARK MATTER

A. Dark Matter Annihilation

Assuming a steady state condition while solving the diffusion equation for the positron as it traversed across the universe, its flux at Earth can be casted into the following semi-analytical form [16, 17]

$$\Phi_{e^+}(E) = \frac{v_{e^+}}{4\pi} f_{e^+}(E) , \quad (1)$$

with v_{e^+} close to the velocity of light c and the function $f_{e^+}(E)$ is given by

$$\begin{aligned} f_{e^+}(E) &= B \frac{1}{b(E)} \int_E^{E_{\max}} dE' I(\lambda_D(E, E')) Q_{\text{ann}}(E') \\ &= B \frac{1}{b(E)} \eta \left(\frac{\rho_{\text{dm}}}{M_{\text{dm}}} \right)^2 \sum \langle \sigma v \rangle_{e^+} \int_E^{E_{\max}} dE' I(\lambda_D(E, E')) \frac{dN_{e^+}}{dE'_{e^+}}, \end{aligned} \quad (2)$$

with $E_{\max} = M_{\text{dm}}$ in the case of annihilating DM, M_{dm} and ρ_{dm} are the mass and the density of the dark matter respectively, and the overall constant B is the boost factor. In Eq.(2) we have expressed the source term Q_{ann} according to

$$Q_{\text{ann}} = \eta \left(\frac{\rho_{\text{dm}}}{M_{\text{dm}}} \right)^2 \sum \langle \sigma v \rangle_{e^+} \frac{dN_{e^+}}{dE_{e^+}}, \quad (3)$$

where $\eta = 1/2(1/4)$ for Majorana or Dirac particle. The summation is over all possible channels that can produce positron in the final state, and dN_{e^+}/dE_{e^+} denotes the spectrum of the positron energy per annihilation in that particular channel. We have suppressed the index labeling the various channels to avoid notation cluttering in the equations. The halo function $I(\lambda_D)$ can be parametrized by

$$I(\lambda_D) = a_0 + a_1 \tanh \left(\frac{b_1 - l}{c_1} \right) \left[a_2 \exp \left(-\frac{(l - b_2)^2}{c_2} \right) + a_3 \right] \quad (4)$$

with $l = \log_{10}(\lambda_D/\text{kpc})$ and the diffusion length $\lambda_D(E, E')$ is given by

$$\lambda_D^2 = 4K_0\tau_E \left[\frac{(E'/\text{GeV})^{\delta-1} - (E/\text{GeV})^{\delta-1}}{\delta - 1} \right]. \quad (5)$$

The constants $a_{0,1,2,3}$, $b_{1,2}$, $c_{1,2}$ and δ , K_0 can be found respectively in Table 2 and Eq.(11) of Ref. [18]. The energy loss rate function $b(E)$ in Eq.(2) is

$$b(E) = \frac{E^2}{(\text{GeV} \times \tau_E)} \quad (6)$$

where $\tau_E = 10^{16}$ seconds. In our analysis, we simply employ the monochromatic annihilation spectrum

$$\frac{dN_{e^+}}{dE_{e^+}}(E) = \frac{1}{M_{\text{dm}}} \delta \left(1 - \frac{E}{M_{\text{dm}}} \right). \quad (7)$$

Analogous formulas for the electron will be omitted here. We only consider the monochromatic e^-e^+ spectrum in this study for simplicity and clarity. We could also add the muon and tau channels in the annihilation, but that would introduce more parameters to complicate our analysis.

B. Decaying Dark Matter

The source term for a decaying dark matter in a particular channel is

$$Q_{\text{dec}} = \frac{1}{\tau_{\text{dm}}} \left(\frac{\rho_{\text{dm}}}{M_{\text{dm}}} \right) \frac{dN_{e^+}}{dE_{e^+}}, \quad (8)$$

where τ_{dm} is the lifetime of the DM and dN_{e^+}/dE_{e^+} is the positron energy spectrum per decay of the DM. The function $f_{e^+}(E)$ is now given by

$$\begin{aligned} f_{e^+}(E) &= \frac{1}{b(E)} \int_E^{E_{\text{max}}} dE' I(\lambda_D(E, E')) Q_{\text{dec}}(E') \\ &= \frac{1}{b(E)} \frac{1}{\tau_{\text{dm}}} \left(\frac{\rho_{\text{dm}}}{M_{\text{dm}}} \right) \int_E^{E_{\text{max}}} dE' I(\lambda_D(E, E')) \frac{dN_{e^+}}{dE'_{e^+}}, \end{aligned} \quad (9)$$

with $E_{\text{max}} = M_{\text{dm}}/2$ for the decaying dark matter and summation over all decay channels is explicit. The flux is the same as in Eq.(1).

In our analysis, we use either a (i) monochromatic decaying spectrum:

$$\frac{dN_{e^+}}{dE_{e^+}}(E) = \frac{2}{M_{\text{dm}}} \delta \left(1 - \frac{2E}{M_{\text{dm}}} \right), \quad (10)$$

or (ii) varying decaying spectrum

$$\frac{dN_{e^+}}{dE_{e^+}}(E) = \frac{80E}{M_{\text{dm}}^2} \left(1 - \frac{2E}{M_{\text{dm}}} \right)^3. \quad (11)$$

The exact form of the varying decaying spectrum is not crucial in our analysis. As long as it is soft it suffices to suit our purpose. We will show that the model that we will use in this work gives an energy spectrum consistent with the above varying spectrum. Analogous formulas for the electron will be omitted as before.

C. Background fluxes

The background electron/positron fluxes from astrophysical sources are believed to be mainly due to Supernova explosions for the primary electrons and from the interactions between the cosmic ray nuclei (mainly proton and helium) and atoms (mainly hydrogen and helium) in the interstellar medium for the secondary electrons and positrons. They are commonly parametrized as [19]

$$\Phi_{e^+}^{\text{bkdg}} = \frac{4.5E^{0.7}}{1 + 650E^{2.3} + 1500E^{4.2}}, \quad (12)$$

$$\begin{aligned} \Phi_{e^-}^{\text{bkdg}} &= \Phi_{e^-}^{\text{bkdg,prim}} + \Phi_{e^-}^{\text{bkdg,sec}} \\ &= \frac{0.16E^{-1.1}}{1 + 11E^{0.9} + 3.2E^{2.15}} + \frac{0.7E^{0.7}}{1 + 110E^{1.5} + 580E^{4.2}}, \end{aligned} \quad (13)$$

where E is in unit of GeV and the unit for the flux is $\text{GeV}^{-1} \text{ cm}^{-2} \text{ s}^{-1} \text{ sr}^{-1}$. We use a normalization of 0.7 so that the flux calculation is consistent with the ATIC data in the low energy range of 20 – 70 GeV.¹

D. Propagation models

To evaluate the halo function $I(\lambda_D)$, we will use the Navarro-Frenk-White (NFW) halo profile with the propagation models “M2”, “Med” and “M1” as parametrized in Ref. [18]. The models “M2”, “Med” and “M1” are characterized by the propagation length in the increasing order. The analysis we will perform in the next section can be straightforwardly repeated for the other popular halo models specified by the Moore profile and the cored isothermal profile.

III. ANALYSIS

Theoretical predictions of the energy spectrum and the positron fraction depend in general on the three input parameters τ_{dm} , $\langle\sigma v\rangle$ and M_{dm} . To achieve the output more or less consistent with the ATIC and PAMELA data, we use $\tau_{\text{dm}} = 1.3 \times 10^{27} \text{ s}$, $B\langle\sigma v\rangle = 5.4 \times 10^{-24} \text{ cm}^3 \text{ s}^{-1}$ and $M_{\text{dm}} = 643 \text{ GeV}$. The energy spectrum for ATIC and the positron fraction for PAMELA are shown in the Fig. 1 and Fig. 2 respectively. We have used the NFW halo model with propagation model “Med” in the figures. From these two plots it is interesting to see that both PAMELA and ATIC data can be fitted simultaneously by the double-action dark matter. We now want to justify this fact more quantitatively using the technique of χ^2 fits.

A. Fitting with PAMELA data only

The PAMELA data shown in Fig. 2 has a rising trend starting from point #9 to #16 which we will be using exclusively in our numerical analysis. The first eight data points are

¹ The normalization of background can vary between 0.6 and 0.8 so that our conclusion of 1-peak-1-bump structure is still valid. If we also vary the normalization in the fits, we found that the best fit for the ATIC data (M2) is similar to the result in row #4 in Table II and the normalization is 0.69, which is close enough to our fixed value of 0.7.

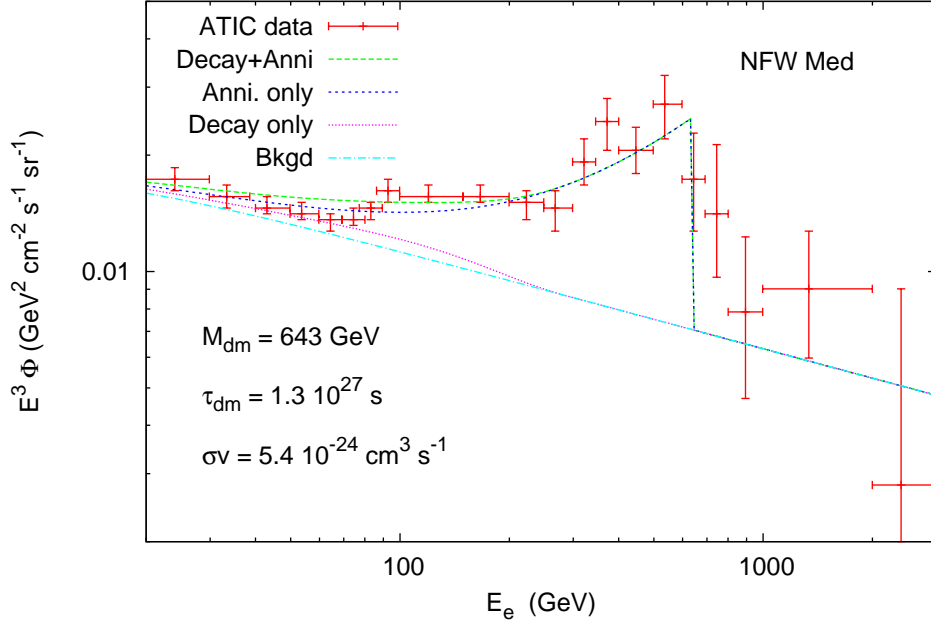


FIG. 1: The spectrum for the ATIC data. The dark matter mass is taken to be 643 GeV, with a monochromatic spectrum for $\text{DM DM} \rightarrow e^+e^-$ annihilation and a soft decaying spectrum of $dN/dE \sim E(1 - 2E/M_{\text{dm}})^3/M_{\text{dm}}^2$ for $\text{DM} \rightarrow e^+e^-X$ decay.

of low energy less than about 10 GeV, where the solar activity of magnetic polarity state is expected to play a significant role in the positron abundance [1]. Both horizontal and vertical errors are explicitly given in the PAMELA publication [1] but only the latter one will be taken into account in our analysis. The parameters used in the analysis are τ_{dm} , $\langle\sigma v\rangle$, and M_{dm} as mentioned earlier. As indicated in previous section, we use a monochromatic electron/positron spectrum for dark matter annihilation, while for decaying dark matter we use either a (i) monochromatic (mono) or (ii) varying spectrum (var). It is denoted by “mono” or “var” in the tables. However, we emphasize that the results do not depend strongly on the exact spectrum as long as it is soft enough. We will show that in some cases the soft spectrum actually fits better than the monochromatic spectrum.

In Table I, we show the fits to the PAMELA data (point #9 to #16) with one or two of the parameters fixed. It can be seen that the “M1” propagation model fits slightly better than “Med” but much better than “M2”. When we vary the mass of dark matter from 200 GeV to 1000 GeV, the goodness of the fit, measured by the χ^2 , is roughly independent of the mass. (It shows a slight better fit when M_{dm} increases, but not of any significance.)

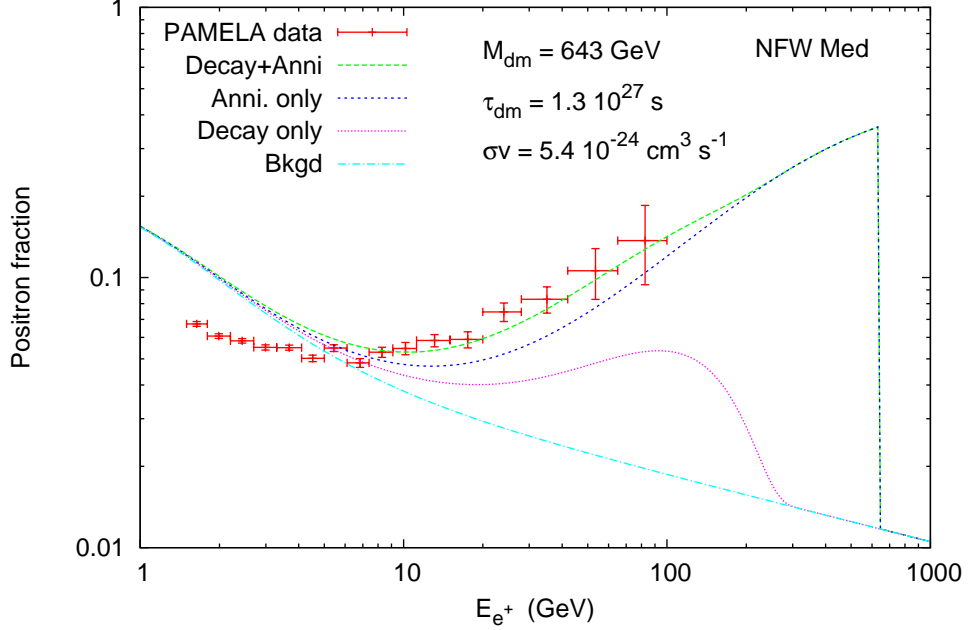


FIG. 2: The positron fraction for the PAMELA data. The dark matter mass is taken to be 643 GeV, with a monochromatic spectrum for $\text{DMDM} \rightarrow e^+e^-$ annihilation and a soft decaying spectrum of $dN/dE \sim E(1 - 2E/M_{\text{dm}})^3/M_{\text{dm}}^2$ for $\text{DM} \rightarrow e^+e^-X$ decay.

Since the PAMELA data did not show any peak structure, the data would not prefer any mass of the dark matter. As long as the propagation diffuses the spectrum or the spectrum itself is soft, it can fit the data well. It is shown in the first three rows in Table I when we used the varying spectrum. The “var” spectrum fits much better than the “mono” spectrum. Thus, the PAMELA data alone do not constrain the mass of dark matter to any significant extent according to this analysis, as long as the mass is heavier than about 200 GeV.

B. Fitting with ATIC data only

The ATIC data exhibits a more interesting feature of one peak plus one hump structure. Thus, we expect that the data prefer some mass range of the dark matter for both annihilation and decaying contributions. By comparing row #4 with #1 to #3 in Table II where the “M2” propagation model is used, we note that with a dark matter about 744 GeV the fit is substantially better with both annihilation and soft decaying contributions included than just either one of them is used. On the other hand, the other two propagation models do

not show such effects. The less diffuse propagation model “M2” fits better than the “Med” and “M1” models.

C. Fitting using both PAMELA and ATIC data

The fits are shown in Table III. Similar to the fits with PAMELA data only, the fits using “M1” propagation model are slightly better than using “Med”, which are in turns much better than “M2”. The fits using “M2” is not good at all, given the fact that χ^2 per d.o.f. is large. This behavior is similar to those fitted to PAMELA data alone.

In the fits with “Med” propagation model, we first fitted with a negligible decaying contribution, i.e., with annihilation contribution only. The best that we can do is $\chi^2 \simeq 59$

TABLE I: Fitting with PAMELA data only. When we fix $\tau_{\text{dm}} = 10^{40}$ s, the contribution from decaying is negligible. Similarly, when we fix $B\langle\sigma v\rangle = 10^{-40}$ cm³ s⁻¹ the contribution from annihilation is negligible. The “mono” means monochromatic spectrum, whereas “var” means varying spectrum for the decaying contribution.

Prop. model	τ_{dm} (s)	$B\langle\sigma v\rangle$ (cm ³ s ⁻¹)	M_{dm} (GeV)	$\chi^2/\#$ d.o.f.	Comments
NFW M2	10^{40} (fixed)	10^{-23}	300 (fixed)	79.6/7	mono
	$0.45 \cdot 10^{27}$	10^{-40} (fixed)	212	18.1/6	var
	$0.55 \cdot 10^{27}$	$0.77 \cdot 10^{-24}$	200 (fixed)	10.1/6	var
NFW Med		$0.15 \cdot 10^{-23}$	250 (fixed)	3.0/7	mono
	fixed	$0.21 \cdot 10^{-23}$	300 (fixed)	2.9/7	mono
	at	$0.37 \cdot 10^{-23}$	400 (fixed)	2.8/7	mono
	10^{40}	$0.83 \cdot 10^{-23}$	600 (fixed)	2.7/7	mono
		$0.15 \cdot 10^{-22}$	800 (fixed)	2.7/7	mono
		$0.22 \cdot 10^{-22}$	1000 (fixed)	2.6/7	mono
NFW M1	fixed	$0.59 \cdot 10^{-24}$	200 (fixed)	3.6/7	mono
	at	$0.36 \cdot 10^{-23}$	500 (fixed)	2.2/7	mono
	10^{40}	$0.70 \cdot 10^{-23}$	700 (fixed)	2.0/7	mono
		$0.14 \cdot 10^{-22}$	1000 (fixed)	1.9/7	mono

at $M_{\text{dm}} \simeq 600 - 700$ GeV. When we also turn on the decaying contribution with a varying spectrum, the χ^2 goes down to 42. This result supports a dark matter that annihilates and also decays with a soft varying spectrum. The best fit is

$$\tau_{\text{dm}} = 0.13 \cdot 10^{28} \text{ s}, \quad B\langle\sigma v\rangle = 0.54 \cdot 10^{-23} \text{ cm}^3 \text{ s}^{-1}, \quad M_{\text{dm}} = 643 \text{ GeV} \quad (14)$$

which has a $\chi^2 \simeq 42/26$ d.o.f. We used this set of fitted parameters in Figs. 1 and 2.

The fits using the “M1” propagation model improve further. Features are similar to the case of “Med”. The best fit using monochromatic annihilation and decaying contributions is (second last row of Table III)

$$\tau_{\text{dm}} = 0.38 \cdot 10^{28} \text{ s}, \quad B\langle\sigma v\rangle = 0.61 \cdot 10^{-23} \text{ cm}^3 \text{ s}^{-1}, \quad M_{\text{dm}} = 745 \text{ GeV} \quad (15)$$

with a $\chi^2 = 38.5/26$ d.o.f. The best fit using monochromatic annihilation but varying spectrum for decaying contribution is (last row of Table III)

$$\tau_{\text{dm}} = 0.33 \cdot 10^{29} \text{ s}, \quad B\langle\sigma v\rangle = 0.54 \cdot 10^{-23} \text{ cm}^3 \text{ s}^{-1}, \quad M_{\text{dm}} = 643 \text{ GeV} \quad (16)$$

with a $\chi^2 = 38.6/26$ d.o.f.

TABLE II: Fitting with ATIC data only. Other details are the same as Table I.

Prop. model	τ_{dm} (s)	$B\langle\sigma v\rangle$ ($\text{cm}^3 \text{ s}^{-1}$)	M_{dm} (GeV)	$\chi^2/\#$ d.o.f.	Comments
NFW M2	10^{40} (fixed)	$0.51 \cdot 10^{-23}$	536	39.5/19	mono
	$0.36 \cdot 10^{27}$	10^{-40} (fixed)	1072	39.5/19	mono
	$1.0 \cdot 10^{26}$	10^{-40} (fixed)	3190	25.3/19	var
	$0.65 \cdot 10^{27}$	$0.80 \cdot 10^{-23}$	744	23.7/18	var
NFW Med	10^{40} (fixed)	$0.78 \cdot 10^{-23}$	745	27.4/19	mono
	$0.32 \cdot 10^{27}$	10^{-40} (fixed)	1490	27.4/19	mono
	$0.25 \cdot 10^{29}$	$0.78 \cdot 10^{-23}$	745	27.4/18	var
NFW M1	10^{40} (fixed)	$0.68 \cdot 10^{-23}$	740	34.2/19	mono
	$0.36 \cdot 10^{27}$	10^{-40} (fixed)	1470	34.2/19	mono
	$0.11 \cdot 10^{27}$	10^{-40} (fixed)	4420	37.6/19	var

TABLE III: Fitting with PAMELA and ATIC data. Other details are the same as previous tables.

Prop. model	τ_{dm} (s)	$B\langle\sigma v\rangle$ ($\text{cm}^3 \text{ s}^{-1}$)	M_{dm} (GeV)	$\chi^2/\#$ d.o.f.	Comments
NFW M2	10^{40} (fixed)	$0.31 \cdot 10^{-23}$	400 (fixed)	297/28	mono
	10^{40} (fixed)	$0.47 \cdot 10^{-23}$	500 (fixed)	281/28	mono
	10^{40} (fixed)	$0.70 \cdot 10^{-23}$	600 (fixed)	269/28	mono
	10^{40} (fixed)	$0.94 \cdot 10^{-23}$	700 (fixed)	275/28	mono
	10^{40} (fixed)	$0.12 \cdot 10^{-22}$	800 (fixed)	284/28	mono
	10^{40} (fixed)	$0.16 \cdot 10^{-22}$	1000 (fixed)	343/28	mono
	10^{40} (fixed)	$0.55 \cdot 10^{-23}$	535	267/27	mono
NFW Med	10^{40} (fixed)	$0.27 \cdot 10^{-23}$	400 (fixed)	96.8/28	mono
	10^{40} (fixed)	$0.42 \cdot 10^{-23}$	500 (fixed)	74.3/28	mono
	10^{40} (fixed)	$0.60 \cdot 10^{-23}$	600 (fixed)	59.1/28	mono
	10^{40} (fixed)	$0.80 \cdot 10^{-23}$	700 (fixed)	59.3/28	mono
	10^{40} (fixed)	$0.10 \cdot 10^{-22}$	800 (fixed)	63.2/28	mono
	10^{40} (fixed)	$0.15 \cdot 10^{-22}$	1000 (fixed)	102/28	mono
	$0.16 \cdot 10^{28}$	$0.62 \cdot 10^{-23}$	745	55.9/26	mono
	$0.13 \cdot 10^{28}$	$0.54 \cdot 10^{-23}$	643	41.9/26	var
NFW M1	10^{40} (fixed)	$0.34 \cdot 10^{-23}$	500 (fixed)	55.3/28	mono
	10^{40} (fixed)	$0.48 \cdot 10^{-23}$	600 (fixed)	41.1/28	mono
	10^{40} (fixed)	$0.64 \cdot 10^{-23}$	700 (fixed)	38.8/28	mono
	10^{40} (fixed)	$0.83 \cdot 10^{-23}$	800 (fixed)	40.0/28	mono
	10^{40} (fixed)	$0.99 \cdot 10^{-23}$	900 (fixed)	66.9/28	mono
	10^{40} (fixed)	$0.12 \cdot 10^{-22}$	1000 (fixed)	66.7/28	mono
	$0.38 \cdot 10^{28}$	$0.61 \cdot 10^{-23}$	745	38.5/26	mono
	$0.33 \cdot 10^{29}$	$0.54 \cdot 10^{-23}$	643	38.6/26	var

IV. A MODEL

We use a TeV right-handed neutrino mass model to present a dark matter candidate that can annihilate and decay. The model can be described by the following interaction Lagrangian [13, 14]

$$\begin{aligned}\mathcal{L}_{\text{int}} = & f_{\alpha\beta} L_{\alpha}^T C i\tau_2 L_{\beta} S_1^+ + g_{1\alpha} N_1 S_2^+ \ell_{\alpha R} + g_{2\alpha} N_2 S_2^+ \ell_{\alpha R} + \text{H.c.} \\ & + M_{N_1} N_1^T C N_1 + M_{N_2} N_2^T C N_2 - V(S_1, S_2)\end{aligned}\quad (17)$$

where $L_{\alpha,\beta}$ and $\ell_{\alpha R}$ are the lepton doublet and singlet respectively with α, β denoting the family indices, $N_{1,2}$ are the two right-handed neutrinos, C is the charge-conjugation operator, and $V(S_1, S_2)$ is the scalar potential for the two complex scalar fields S_1 and S_2 that containing a term $\lambda_s (S_1^+ S_2^-)^2$. Note that $f_{\alpha\beta}$ is antisymmetric under the interchange of the family indices. The original model in Ref. [13] contains only one N_1 , but the improvement in Ref. [14] by adding another N_2 makes the model consistent with the neutrino oscillation data. For simplicity we shall only describe the lighter right-handed neutrino N_1 (denoted simply by N in what follows), which is in the TeV mass range, as far as dark matter is concerned. It has been shown [14] that N can be a dark matter candidate. The annihilation $NN \rightarrow e^+ e^-$ can go through t - and u -channel diagrams with an intermediate S_2^+ (see Fig. 3(a)) with the rate given by

$$\begin{aligned}\sigma v_{\text{rel}} = & \frac{g_{1e}^4}{64\pi} \frac{1}{s} \int_{-1}^1 dx \left\{ \frac{s^2(1 - \beta_N x)^2}{4(M_N^2 - M_{S_2}^2 - \frac{s}{2}(1 - \beta_N x))^2} + \frac{s^2(1 + \beta_N x)^2}{4(M_N^2 - M_{S_2}^2 - \frac{s}{2}(1 + \beta_N x))^2} \right. \\ & \left. - \frac{2M_N^2 s}{(M_N^2 - M_{S_2}^2 - \frac{s}{2}(1 - \beta_N x))(M_N^2 - M_{S_2}^2 - \frac{s}{2}(1 + \beta_N x))} \right\}\end{aligned}\quad (18)$$

where $\beta_N = (1 - 4M_N^2/s)^{1/2}$. As $\beta_N \rightarrow 0$, the above annihilation rate vanishes. This is expected for the annihilation rate for identical Majorana fermions is P-wave suppressed [20]. When the center of mass energy \sqrt{s} is slightly above the threshold of $2M_N$, the annihilation electron/positron energy spectrum is almost a monochromatic one. We show in Fig. 4 the annihilation cross section versus the right-handed neutrino mass for various values of the scalar mass, taking the center-of-mass energy \sqrt{s} at which $v_{\text{rel}} \approx 10^{-3}$. The plot demonstrates the P-wave suppression. Therefore, a large boost factor of order $O(10^7)$ is needed to fit the data in this model. However, this suppression might not be taken literally. If one is willing to extend the model by introducing new long range force among the dark

matter, the Sommerfeld enhancement for P-wave annihilation can be significantly larger than the S-wave case [21].

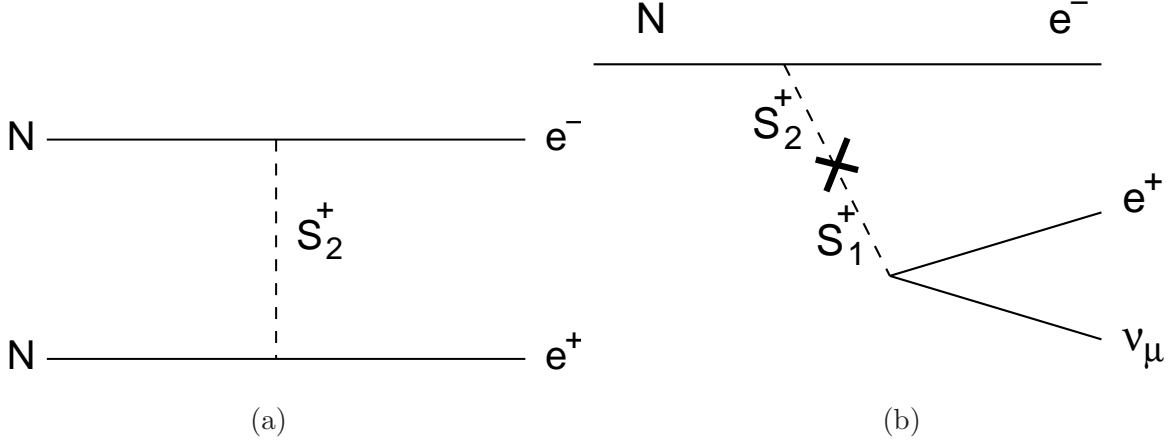


FIG. 3: Feynman diagrams for (a) annihilation $NN \rightarrow e^-e^+$ and (b) decay $N \rightarrow e^-e^+\nu_\mu$.

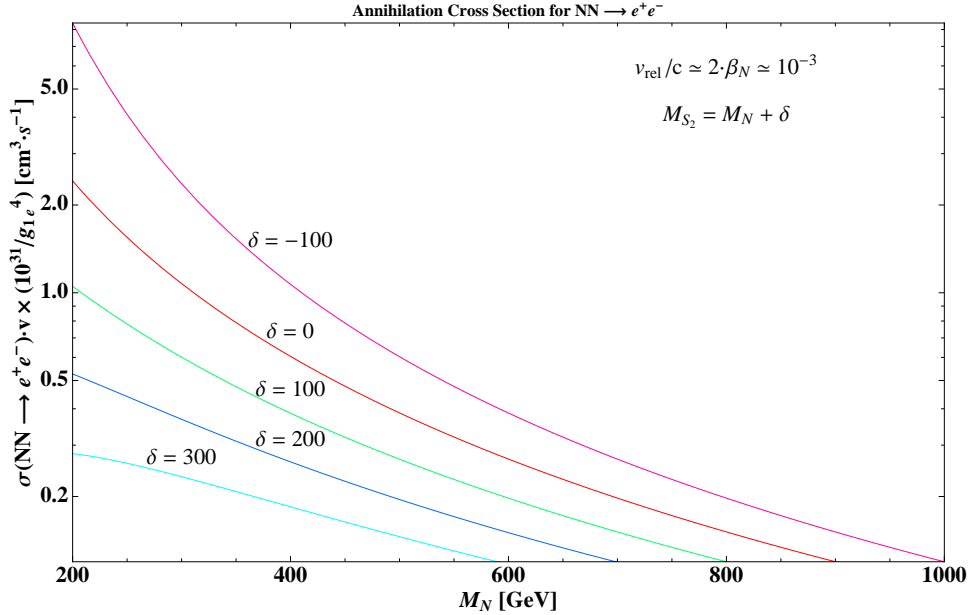


FIG. 4: Annihilation cross section versus the right-handed neutrino mass for various values of the scalar mass at a center-of-mass energy \sqrt{s} when the $v_{\text{rel}} \approx 10^{-3}$.

In Refs. [13, 14], the N is assumed stable by imposing a Z_2 parity. Here we introduce a small violation of this parity by adding a term $\epsilon S_1^+ S_2^- + \text{H.c.}$ to the scalar potential, where $\epsilon \sim (1 \text{ eV})^2$, which is of the order of the square of neutrino mass. The decay of N can then

go through a Feynman diagram shown in Fig. 3(b).² An order of magnitude estimate of the decay width of the N can be given as

$$\Gamma_N \sim g_{1e}^2 f_{12}^2 \epsilon^2 M_N / M_{S_2}^4 . \quad (19)$$

Taking typical values of the couplings [14] ($g_{1e} \sim 10^{-1}$, $f_{12} \sim 10^{-2}$, $M_N \sim M_{S_2} \sim \text{TeV}$), the lifetime of N is roughly

$$\tau_N \sim 10^{26} \left(\frac{\text{eV}^2}{\epsilon} \right)^2 \text{ sec} . \quad (20)$$

It is interesting to see that when ϵ is of the order of the neutrino mass squared, the amount of violation of the Z_2 parity is in the right order to fit the data. We calculate the normalized energy spectrum of the decay $N \rightarrow e^- e^+ \nu_\mu$ shown in Fig. 5, where the approximate spectrum $80x(1-2x)^3$ with $x = E/M_{\text{dm}}$ is also shown. The figure justifies the approximation of the energy spectrum that we have used in our analysis given in the previous section. Note that the exact form is not crucial in the fits as long as the spectrum is soft. In this model, the decay and annihilation of the dark matter are pure leptonic. It will not give enhancement to the \bar{p} flux.

² There is another decay channel $N \rightarrow e^- \mu^+ \nu_e$ given the same couplings. The lifetime will be shorten by a factor of two, but it does not affect our order-of-magnitude estimate.

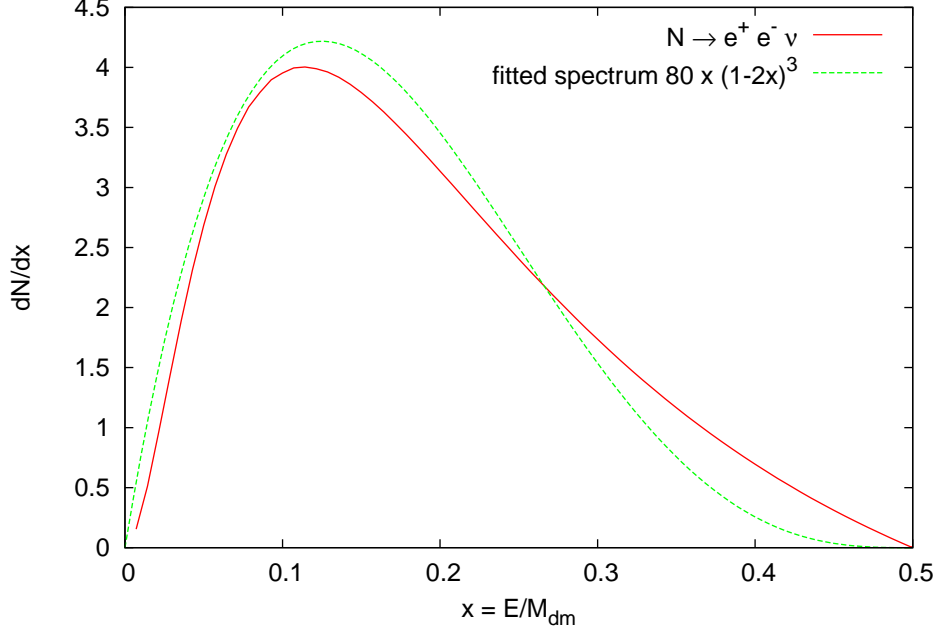


FIG. 5: Normalized energy spectrum $1/\Gamma d\Gamma/dx$ with $x = E/M_{\text{dm}}$ for the decay $N \rightarrow e^- e^+ \nu_\mu$ and the approximation $80x(1 - 2x)^3$.

V. CONCLUSION

We have pointed out a 2-bump (or 1 peak plus 1 hump) structure in the ATIC data. If this feature can be sustained it cannot be explained by dark matter annihilation or decay alone. It can be either a two-component dark matter or the dark matter can undergo both annihilation and decay at the same time. We have shown that such a double-action dark matter can fit better to the ATIC and PAMELA data simultaneously than just annihilation or decay alone. We have employed a TeV right-handed neutrino model to illustrate the idea. The original model only allows dark matter annihilation, but here we have introduced a small breaking of the Z_2 parity at the order of the neutrino mass squared. With such a coincident size of Z_2 breaking one can explain the long lifetime required to fit the data. This indicates there may be intricate connection between neutrino mass problem with dark matter physics. We close with a few comments.

- The model of TeV right-handed neutrino can account for the neutrino mass and oscillation pattern [13, 14]. It is also consistent with lepton-flavor violation. The lightest

of the right-handed neutrino can be a dark matter candidate and its relic density can account for the observed dark matter density.

- Reference [14] showed that the model can be made consistent with existing neutrino oscillation data by tuning the parameters of the model. If so there would also be the muon and tau channels in the annihilation. The electron/positron spectrum would contain the monochromatic part and the continuous part from muon and tau decays. The χ^2 analysis would be much more involved and beyond the scope of this paper.
- The decay and annihilation of the dark matter are pure leptonic. It will not give enhancement to the \bar{p} flux.
- The Z_2 parity violation parameter ϵ that we introduced is, by accident, at the order of the square of the neutrino mass.
- The prediction for the gamma-ray flux mainly comes from the bremsstrahlung off the electron/positron.
- Since the TeV right-handed neutrino has no appreciable coupling to quarks or gluons, the scattering cross section with nuclei is negligible. Thus, the sun or the Earth will not capture any large amount of dark matter, and so no enhancement to the neutrino flux coming from the core of the sun.
- Either annihilation or decay alone cannot explain the probable 1-peak plus 1-hump structure in the ATIC data. We have shown that a dark matter that can annihilate and decay simultaneously can explain the ATIC and PAMELA data at the same time.

Dark matter interpretation for the PAMELA and ATIC experiments is exciting since it implies new physics beyond the Standard Model. However, one should keep in mind that a yet unidentified astrophysical object such as a nearby pulsar or micro-quasar could be a primary source as well. Furthermore, many models are capable to explain the excess anomaly. PAMELA is extending the spectra measurement to higher energy of about 300 GeV for positrons and 500 GeV for electrons. New data is also expected soon from the FERMI satellite for the diffuse Galactic cosmic γ -ray spectrum. These future developments will certainly help to discriminate models and unravel the true nature of the anomaly seen thus far. More excitements are waiting ahead of us!

Acknowledgment

We thank Wai-Yee Keung and Vernon Barger for a useful communication. The work was supported in parts by the NSC of Taiwan under grant no. 96-2628-M-007-002-MY3, the NCTS, the Boost Program of NTHU, and the WCU program through the KOSEF funded by the MEST (R31-2008-000-10057-0).

-
- [1] O. Adriani *et al.*, [PAMELA Collaboration], Nature 458, 607 (2009).
 - [2] S. W. Barwick *et al.*, [HEAT Collaboration], Astrophys. J. **482**, L191 (1997) [arXiv:astro-ph/9703192].
 - [3] M. Aguilar *et al.*, [AMS-01 Collaboration], Phys. Lett. B **646**, 145 (2007) [arXiv:astro-ph/0703154].
 - [4] O. Adriani *et al.*, [PAMELA Collaboration], Phys. Rev. Lett. 102, 051101 (2009).
 - [5] J. Chang *et al.*, [ATIC Collaboration], Nature 456, 362 (2008).
 - [6] S. Torii *et al.*, arXiv:0809.0760 [astro-ph].
 - [7] L. Bergstrom, T. Bringmann and J. Edsjo, Phys. Rev. D **77**, 103520 (2008) [arXiv:0808.3725 [astro-ph]],
M. Cirelli and A. Strumia, arXiv:0808.3867 [astro-ph],
M. Cirelli, M. Kadastik, M. Raidal and A. Strumia, arXiv:0809.2409 [hep-ph],
V. Barger, W. Y. Keung, D. Marfatia and G. Shaughnessy, Phys. Lett. B **672**, 141 (2009) [arXiv:0809.0162 [hep-ph]],
J. Hisano, M. Kawasaki, K. Kohri and K. Nakayama, arXiv:0810.1892 [hep-ph],
J. H. Huh, J. E. Kim and B. Kyae, arXiv:0809.2601 [hep-ph],
M. Masip and I. Mastromatteo, JCAP **0812**, 003 (2008) [arXiv:0810.4468 [hep-ph]],
P. D. Serpico, Phys. Rev. D **79**, 021302 (2009) [arXiv:0810.4846 [hep-ph]],
A. E. Nelson and C. Spitzer, arXiv:0810.5167 [hep-ph],
T. Bringmann, arXiv:0810.5304 [hep-ph],
I. Cholis, D. P. Finkbeiner, L. Goodenough and N. Weiner, arXiv:0810.5344 [astro-ph],
Y. Nomura and J. Thaler, arXiv:0810.5397 [hep-ph],
R. Harnik and G. D. Kribs, arXiv:0810.5557 [hep-ph],

D. Feldman, Z. Liu and P. Nath, arXiv:0810.5762 [hep-ph],
 K. Ishiwata, S. Matsumoto and T. Moroi, arXiv:0811.0250 [hep-ph],
 Y. Bai and Z. Han, arXiv:0811.0387 [hep-ph],
 P. J. Fox and E. Poppitz, arXiv:0811.0399 [hep-ph],
 E. Ponton and L. Randall, arXiv:0811.1029 [hep-ph],
 S. Baek and P. Ko, arXiv:0811.1646 [hep-ph],
 A. Morselli and I. V. Moskalenko, arXiv:0811.3526 [astro-ph],
 I. Cholis, G. Dobler, D. P. Finkbeiner, L. Goodenough and N. Weiner, arXiv:0811.3641 [astro-ph],
 K. M. Zurek, arXiv:0811.4429 [hep-ph],
 M. Taoso, S. Ando, G. Bertone and S. Profumo, arXiv:0811.4493 [astro-ph],
 J. Hisano, M. Kawasaki, K. Kohri and K. Nakayama, arXiv:0812.0219 [hep-ph],
 E. J. Chun and J. C. Park, arXiv:0812.0308 [hep-ph],
 J. Liu, P. f. Yin and S. h. Zhu, arXiv:0812.0964 [astro-ph],
 M. Pohl, arXiv:0812.1174 [astro-ph],
 R. Allahverdi, B. Dutta, K. Richardson-McDaniel and Y. Santoso, arXiv:0812.2196 [hep-ph],
 K. Hamaguchi, S. Shirai and T. T. Yanagida, arXiv:0812.2374 [hep-ph],
 D. Hooper, A. Stebbins and K. M. Zurek, arXiv:0812.3202 [hep-ph],
 K. J. Bae, J. H. Huh, J. E. Kim, B. Kyae and R. D. Viollier, arXiv:0812.3511 [hep-ph],
 J. Lavalle, arXiv:0812.3576 [astro-ph],
 P. Grajek, G. Kane, D. Phalen, A. Pierce and S. Watson, arXiv:0812.4555 [hep-ph],
 J. H. Huh, J. E. Kim and B. Kyae, arXiv:0812.5004 [hep-ph],
 X. J. Bi, P. H. Gu, T. Li and X. Zhang, arXiv:0901.0176 [hep-ph],
 S. C. Park and J. Shu, arXiv:0901.0720 [hep-ph],
 I. Gogoladze, R. Khalid, Q. Shafi and H. Yuksel, arXiv:0901.0923 [hep-ph],
 Q. H. Cao, E. Ma and G. Shaughnessy, arXiv:0901.1334 [hep-ph],
 E. Nezri, M. H. G. Tytgat and G. Vertongen, arXiv:0901.2556 [hep-ph],
 J. Mardon, Y. Nomura, D. Stolarski and J. Thaler, arXiv:0901.2926 [hep-ph],
 D. J. Phalen, A. Pierce and N. Weiner, arXiv:0901.3165 [hep-ph],
 J. Hisano, M. Kawasaki, K. Kohri, T. Moroi and K. Nakayama, arXiv:0901.3582 [hep-ph],
 D. Hooper and K. Zurek, arXiv:0902.0593 [hep-ph],

- H.-S. Goh, L. J. Hall and P. Kumar, arXiv:0902.0814 [hep-ph],
- M. Ibe, Y. Nakayama, H. Murayama and T. T. Yanagida, arXiv:0902.2914 [hep-ph],
- R. Allahverdi, B. Dutta, K. Richardson-McDaniel and Y. Santoso, arXiv:0902.3463 [hep-ph].
- [8] C. R. Chen, F. Takahashi and T. T. Yanagida, Phys. Lett. B **671**, 71 (2009) [arXiv:0809.0792 [hep-ph]],
- C. R. Chen and F. Takahashi, JCAP **0902**, 004 (2009) [arXiv:0810.4110 [hep-ph]],
- P. f. Yin, Q. Yuan, J. Liu, J. Zhang, X. j. Bi and S. h. Zhu, Phys. Rev. D **79**, 023512 (2009) [arXiv:0811.0176 [hep-ph]],
- C. R. Chen, F. Takahashi and T. T. Yanagida, arXiv:0811.0477 [hep-ph],
- K. Hamaguchi, E. Nakamura, S. Shirai and T. T. Yanagida, arXiv:0811.0737 [hep-ph],
- A. Ibarra and D. Tran, arXiv:0811.1555 [hep-ph],
- C. R. Chen, M. M. Nojiri, F. Takahashi and T. T. Yanagida, arXiv:0811.3357 [astro-ph],
- E. Nardi, F. Sannino and A. Strumia, JCAP **0901**, 043 (2009) [arXiv:0811.4153 [hep-ph]],
- S. D. L. Amigo, W. Y. L. Cheung, Z. Huang and S. P. Ng, arXiv:0812.4016 [hep-ph],
- C. R. Chen, K. Hamaguchi, M. M. Nojiri, F. Takahashi and S. Torii, arXiv:0812.4200 [astro-ph],
- F. Takahashi and E. Komatsu, arXiv:0901.1915 [astro-ph],
- K. Hamaguchi, F. Takahashi and T. T. Yanagida, arXiv:0901.2168 [hep-ph],
- C. H. Chen, C. Q. Geng and D. V. Zhuridov, arXiv:0901.2681 [hep-ph],
- F. Chen, J. M. Cline and A. R. Frey, arXiv:0901.4327 [hep-ph],
- X. Chen, arXiv:0902.0008 [hep-ph],
- L. Covi and J. E. Kim, arXiv:0902.0769 [astro-ph.CO],
- K. J. Bae and B. Kyae, arXiv:0902.3578 [hep-ph].
- [9] H. B. Hu, Q. Yuan, B. Wang, C. Fan, J. L. Zhang and X. J. Bi, arXiv:0901.1520 [astro-ph].
- [10] D. Hooper, P. Blasi and P. D. Serpico, JCAP **0901**, 025 (2009) [arXiv:0810.1527 [astro-ph]],
- H. Yuksel, M. D. Kistler and T. Stanev, arXiv:0810.2784 [astro-ph].
- J. Hall and D. Hooper, arXiv:0811.3362 [astro-ph],
- S. Profumo, arXiv:0812.4457 [astro-ph],
- K. Ioka, arXiv:0812.4851 [astro-ph].
- [11] J. Hisano, S. Matsumoto, M. M. Nojiri and O. Saito, Phys. Rev. D **71**, 063528 (2005) [arXiv:hep-ph/0412403],

- N. Arkani-Hamed, D. P. Finkbeiner, T. Slatyer and N. Weiner, Phys. Rev. D **79**, 015014 (2009) [arXiv:0810.0713 [hep-ph]],
- M. Ibe, H. Murayama and T. T. Yanagida, arXiv:0812.0072 [hep-ph],
- M. Lattanzi and J. I. Silk, arXiv:0812.0360 [astro-ph],
- W. L. Guo and Y. L. Wu, arXiv:0901.1450 [hep-ph].
- J. March-Russell, S. M. West, D. Cumberbatch and D. Hooper, JHEP **0807**, 058 (2008) [arXiv:0801.3440 [hep-ph]].
- J. D. March-Russell and S. M. West, arXiv:0812.0559 [astro-ph].
- [12] L. Bergstrom, G. Bertone, T. Bringmann, J. Edsjo and M. Taoso, arXiv:0812.3895 [astro-ph],
- P. Meade, M. Papucci and T. Volansky, arXiv:0901.2925 [hep-ph],
- K. Ishiwata, S. Matsumoto and T. Moroi, arXiv:0811.4492 [astro-ph],
- J. Zhang, X. J. Bi, J. Liu, S. M. Liu, P. f. Yin, Q. Yuan and S. H. Zhu, arXiv:0812.0522 [astro-ph],
- W. de Boer, arXiv:0901.2941 [hep-ph].
- [13] L. M. Krauss, S. Nasri and M. Trodden, Phys. Rev. D **67**, 085002 (2003) [arXiv:hep-ph/0210389].
- [14] K. Cheung and O. Seto, Phys. Rev. D **69**, 113009 (2004) [arXiv:hep-ph/0403003].
- [15] M. Aoki, S. Kanemura and O. Seto, Phys. Rev. Lett. **102**, 051805 (2009) [arXiv:0807.0361 [hep-ph]].
- [16] T. Delahaye, R. Lineros, F. Donato, N. Fornengo and P. Salati, Phys. Rev. D **77**, 063527 (2008) [arXiv:0712.2312 [astro-ph]].
- [17] J. Hisano, S. Matsumoto, O. Saito and M. Senami, Phys. Rev. D **73**, 055004 (2006) [hep-ph/0511118]
- [18] M. Cirelli, R. Franceschini and A. Strumia, Nucl. Phys. B **800**, 204 (2008) [arXiv:0802.3378 [hep-ph]].
- [19] E. A. Baltz and J. Edsjo, Phys. Rev. D **59**, 023511 (1999) [astro-ph/9808243].
- [20] H. Goldberg, Phys. Rev. Lett. **50**, 1419 (1983).
- [21] R. Iengo, arXiv:0903.0317 [hep-ph], arXiv:0902.0688 [hep-ph]; S. Cassel, arXiv:0903.5307 [hep-ph].